PHILOSOPHICAL TRANSACTIONS OF THE ROYAL SOCIETY B BIOLOGICAL SCIENCES

Resonance in a Model of a Mammalian Neuron

J. L. Hindmarsh and R. M. Rose

Phil. Trans. R. Soc. Lond. B 1994 **346**, 151-163
doi: 10.1098/rstb.1994.0138

Resonance in a model of a mammalian neuron

J. L. HINDMARSH[1] AND R. M. ROSE[2]

School of Mathematics[1] and Department of Physiology[2], University of Wales College of Cardiff, Cathays Park, Cardiff CF1 1SS, U.K.

SUMMARY

In this paper we show that for a small range of voltages the model described in the previous paper (Hindmarsh & Rose *Phil. Trans. R. Soc. Lond.* B **346**, 129–150 (1994*a*)) will generate damped oscillations in response to a negative current pulse. As a consequence the cell has the property that it can be driven into bursting by periodic sinusoidal inputs close to the resonant frequency. The main objective of this paper is to analyse this resonant behaviour using the model of the model introduced in the previous paper. We derive analytical expressions which closely approximate the nonlinear resonance observed in the physiological model driven by a periodic sinusoidal input. This leads to the conclusion that resonance could play a role in synaptic transmission at relay nuclei in the mammalian brain.

1. INTRODUCTION

In the previous paper (Hindmarsh & Rose 1994*a*) we described a model of a mammalian neuron which showed rebound bursting following a hyperpolarizing current step. In this paper we examine the response of the model to periodic external currents of small amplitude.

From the bifurcation diagram (figure 1) we see that for a limited range of constant external currents the system has a stable equilibrium point (EP), an unstable limit cycle, and a stable limit cycle. The stable EP has associated with it a pair of complex conjugate eigenvalues, and typically the state paths approach the EP in a spiral fashion. By analogy with the damped harmonic oscillator we expect that at such an EP the cell could resonate to a periodic forcing function. Close to the resonant frequency a periodic input of sufficient amplitude could drive the cell into continuous bursting.

In our model, rebound oscillations and resonance result from the addition of a transient inward Ca^{2+} current, I_T, and a Ca^{2+}-activated K^+ current, $I_{KCa(T)}$ to the Hodgkin–Huxley equations. In the inner hair cells of lower Vertebrates, resonance also occurs through the interaction of an inward Ca^{2+} current and a Ca^{2+}-activated K^+ current (Fettiplace 1987). The linear response characteristics of these cells have been represented using equivalent electrical circuits (Ashmore & Attwell 1985; Crawford & Fettiplace 1981). These circuits are a development of earlier work on the subthreshold oscillatory responses of the squid axon using the linearized Hodgkin–Huxley equations (Chandler *et al.* 1962; Mauro *et al.* 1970). In this paper we take a different approach to see the consequences of the nonlinear nature of the equations. We examine both the response of the system to signals of varying frequency but fixed amplitude, and, for different frequencies, the amplitude required to drive the cells from equilibrium to bursting.

The possibility that mammalian neurons showing rebound oscillations might respond preferentially to certain input frequencies has been emphasized in a recent review of the intrinsic properties of these cells (Llinás 1988). The aim of this paper is to make these ideas more precise. We will show how resonance can be measured experimentally in cells showing rebound bursting. The predicted tuning curve has a sharp asymmetry which we will describe analytically using the model of the model introduced in the previous paper (Hindmarsh & Rose 1994*a*).

Although our results apply to sinusoidal inputs (i.e. this is an experimental prediction), it is likely that cells of this type will also resonate to synaptic current inputs. The possibility that small synaptic currents could drive the cell into a distinct bursting state will be commented upon further in the following paper (Hindmarsh & Rose 1994*b*).

2. RESONANCE

In the previous paper (Hindmarsh & Rose 1994*a*) we plotted a bifurcation diagrams for the system:

$$\left.\begin{aligned} \dot{v} &= C^{-1}\{-g_L(v-v_L) - g_K n_\infty^4(v)(v-v_K) \\ &\quad - g_T m_{T_\infty}(v) h_T (v-v_{Ca}) \\ &\quad - g_{KCa(T)}\left(\frac{c}{K_{Ca(T)}+c}\right)(v-v_K) \\ &\quad + I_0 + I + I(t)\}, \\ \dot{h}_T &= \tau_{h_T}^{-1}(h_{T_\infty}(v) - h_T), \\ \dot{c} &= -k g_T m_{T_\infty}(v) h_T (v-v_{Ca}) - k_{Ca} c. \end{aligned}\right\} \quad (1)$$

Phil. Trans. R. Soc. Lond. B (1994) **346**, 151–163
Printed in Great Britain

These diagrams were classified as Types A–D. Although it would be desirable to investigate resonance for all four types, we will restrict the analytical discussion to Type D because we have already introduced a simplified model for this case (Hindmarsh & Rose 1994*a*) and because the threshold tuning curve, to be discussed below, shows an interesting asymmetry in this case. In the last section we will comment on numerical calculations for cells with bifurcation diagrams of Types A and B.

Using the parameter values given in Appendix 1 of Hindmarsh & Rose (1994*a*), part of a Type D bifurcation diagram is reproduced in figure 1*a*. For values of the bifurcation parameter, the external current, between $I = I_2$ and $I = I_3'$, the system has a stable EP (as well as an unstable and stable limit cycle). These EPs corresponding to points on the dotted line of the diagram, have membrane potentials in a narrow range. At these EPs, the eigenvalues of the linear approximation matrix are of the form $-\alpha \pm \imath\beta, -\gamma$ where $\alpha, \beta, \gamma > 0$. The complex conjugate pair of eigenvalues with negative real part correspond to damped oscillatory behaviour of the cell on return to equilibrium. In figure 1*b* the system is in the initial state:

$$\boldsymbol{v}_0 = \begin{pmatrix} v_0 \\ h_{T0} \\ c_0 \end{pmatrix} = \begin{pmatrix} -63.3 \\ 0.033 \\ 0.059 \end{pmatrix},$$

with $I_0 = -1.35\,\mu\mathrm{A\,cm^{-2}}$ as in the previous paper (Hindmarsh & Rose 1994*a*) and $I + I(t) = 0\,\mu\mathrm{A\,cm^{-2}}$. We now apply a strong negative current pulse $I(t) = -0.6\,\mu\mathrm{A\,cm^{-2}}$ of short duration, $\tau = 0.5$ ms. The effect of this pulse is to decrease the membrane potential by approximately $I\tau$ mV, that is 0.3 mV, and leave the other variables unchanged. The state of the system is now:

$$\boldsymbol{v}_1 = \boldsymbol{v}_0 + \begin{pmatrix} -0.3 \\ 0 \\ 0 \end{pmatrix}.$$

Following the termination of the pulse the state of the system returns to the resting point. The time course of the membrane potential during this return to the EP may be computed using the linear approximation at $\boldsymbol{v}_0$ and taking advantage of the canonical form (Hindmarsh & Rose 1994*a*). The subsequent state is

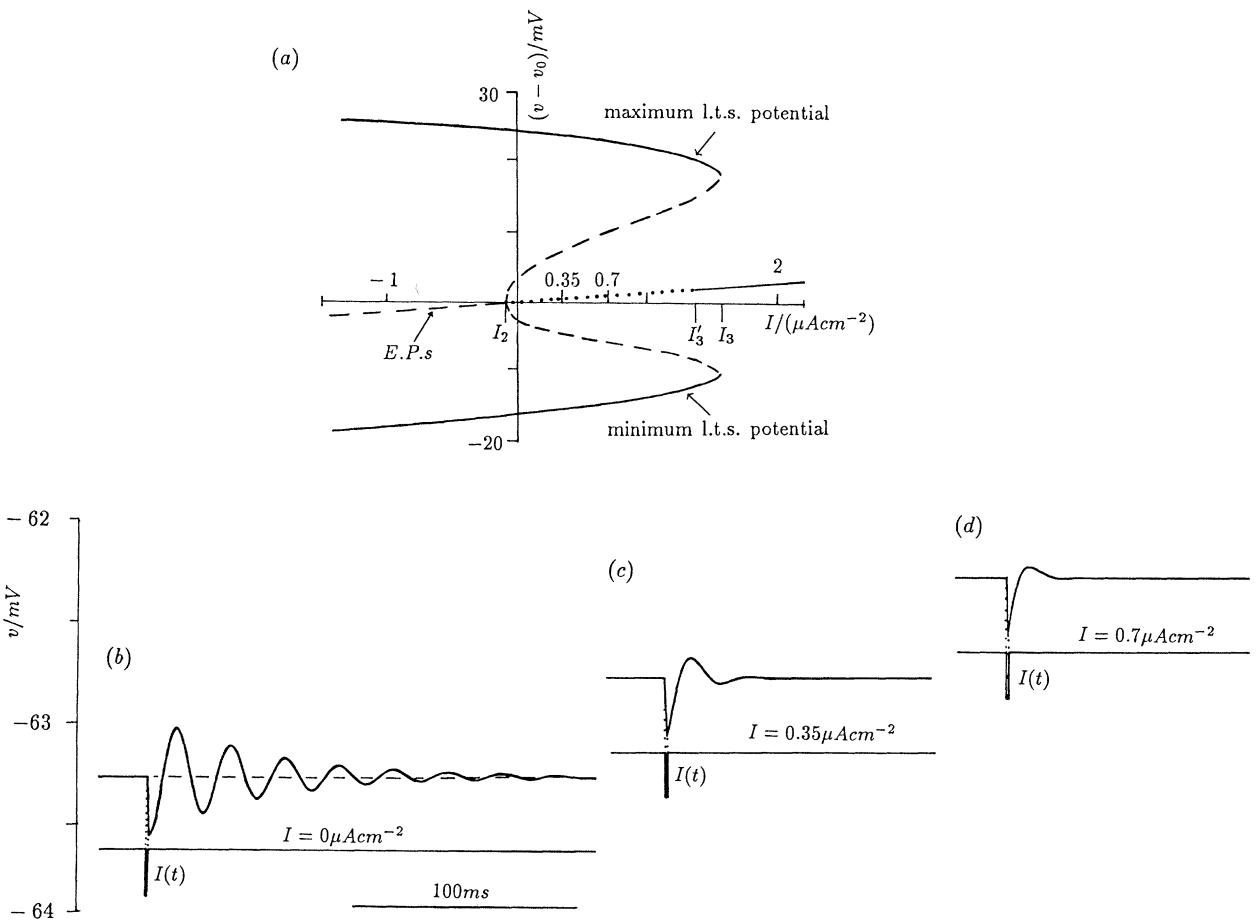

Figure 1. (*a*) $(I, v - v_0)$ bifurcation diagram for the standard physiological model, whose parameter values are given in Appendix 1 of Hindmarsh & Rose (1994*a*). For explanation see text. (*b–d*) Responses of the linearized approximation to equations (1), calculated using equations (2) (with the same parameter values as in (*a*)), to current pulses of amplitude $-0.6\,\mu\mathrm{A}^{-2}$ applied for $\tau = 0.5$ ms at EPs with resting potential v_0 and external current I given by: (*b*) $v_0 = -63.256$ mV, $I = 0\,\mu\mathrm{A\,cm^{-2}}$, (*c*) $v_0 = -62.775$ mV, $I = 0.35\,\mu\mathrm{A\,cm^{-2}}$ and (*d*) $v_0 = -63.28$ mV, $I = 0.7\,\mu\mathrm{A\,cm^{-2}}$. The differences between these analytical solutions and those obtained by numerical integration of equations (1) are negligible.

given by

$$\boldsymbol{v}(t) = \boldsymbol{T}^{-1}\boldsymbol{x}(t) + \boldsymbol{v}_0, \tag{2}$$

where

$$\boldsymbol{x}(t) = \begin{pmatrix} e^{-\alpha t}\cos\beta t & e^{-\alpha t}\sin\beta t & 0 \\ -e^{-\alpha t}\sin\beta t & e^{-\alpha t}\cos\beta t & 0 \\ 0 & 0 & e^{-\gamma t} \end{pmatrix} \boldsymbol{x}_0,$$

and

$$\boldsymbol{x}_0 = \boldsymbol{T}(\boldsymbol{v}_1 - \boldsymbol{v}_0).$$

The timecourse of the membrane potential, $v(t)$, computed using equation (2), with parameter values given in Appendix 2 of Hindmarsh & Rose (1994*a*), is shown in figure 1*b*. The timecourse computed using equations (1) was almost identical (not shown). This similarity of the two time courses confirms the validity of the linear approximation.

Responses to a current pulse of the same amplitude and duration for more positive values of the external current, I, are shown in figures 1*c* and 1*d*. These responses were also computed using equation (2) with values for $\boldsymbol{T}$, $\boldsymbol{T}^{-1}$, α, β and γ appropriate for the new EP. Note that as the EP is moved further from the bifurcation point, the responses become more damped. This is mainly caused by an increase in the value of damping α. Note that similar strongly damped responses may also be obtained in the case of a system with a supercritical bifurcation diagram such as that shown in figure 2*a* of the previous paper (Hindmarsh & Rose 1994*a*) provided that the resting point is chosen sufficiently close to the bifurcation point.

Similar responses to those shown in figure 1 may be obtained if we replace the current pulse by a synaptic current of the form $I_{\mathrm{syn}}(t) = g_{\mathrm{syn}}(t)(v - v_{\mathrm{syn}})$ and apply a pulsatile change in $g_{\mathrm{syn}}(t)$. These responses can be obtained with v_{syn} as closely as 4–5 mV negative to v_0, as might be appropriate for a $GABA_A$ inhibitory synapse. However small amplitude damped oscillatory postsynaptic potentials with a similar timecourse to the response shown in figure 1*b*, have not to our knowledge been reported in the literature.

The damped oscillations of figure 1 suggest that if a cell were at rest at one of these EPs, then its response to a periodic input would increase as the input frequency approached the oscillation frequency. That is, the cell would exhibit resonant behaviour, which should be more pronounced for small values of the damping α. In this paper we will use sinusoidal input currents. Similar results can be obtained using current pulses (not shown). We also apply the analysis at the EP shown in figure 1*b* where the damped oscillation was most pronounced. In § 9 we will show that there is still significant resonance at the EPs shown in figures 1*c* and 1*d*, where the current pulse responses are more strongly damped.

3. THE THRESHOLD CURVE (TC)

We now consider the model described by equations (1) with $I(t) = \bar{I}\cos\omega t$. These are:

$$\left.\begin{aligned} \dot{v} = C^{-1}\{&-g_{\mathrm{L}}(v - v_{\mathrm{L}}) - g_{\mathrm{K}} n_{\infty}^4(v)(v - v_{\mathrm{K}}) \\ &- g_{\mathrm{T}} m_{\mathrm{T}_\infty}(v) h_{\mathrm{T}}(v - v_{\mathrm{Ca}}) \\ &- g_{\mathrm{KCa(T)}}\left(\frac{c}{K_{\mathrm{Ca(T)}} + c}\right)(v - v_{\mathrm{K}}) \\ &+ I_0 + I + \bar{I}\cos\omega t\}, \\ \dot{h}_{\mathrm{T}} = \tau_{h_{\mathrm{T}}}^{-1}&(h_{\mathrm{T}_\infty}(v) - h_{\mathrm{T}}), \\ \dot{c} = -k&g_{\mathrm{T}} m_{\mathrm{T}_\infty}(v) h_{\mathrm{T}}(v - v_{\mathrm{Ca}}) - k_{\mathrm{Ca}} c. \end{aligned}\right\} \tag{3}$$

We examine responses at the EP $v_0 = -63.3$ mV with $I_0 = -1.35\ \mu\mathrm{A\,cm^{-2}}$ and $I = 0$.

The curve shown in figure 2*a* was obtained by finding, for each value of frequency, $f = 1000\omega/(2\pi)$ Hz, the (threshold) amplitude $\bar{I}$, of a periodic input $\bar{I}\cos\omega t$, which is just sufficient to drive the system from the stable EP to the stable limit cycle. We call these curves threshold curves (TCs). Note that when in the stable limit cycle the cell generates low threshold spikes (LTS), which in the full six-dimensional system (see Hindmarsh & Rose 1994*a*, equations (4)) will generate periodic bursts of fast action potentials. Examples of reaching the stable limit cycle for an input amplitude above the TC, and of failure to reach the stable limit cycle for an input amplitude below the TC are shown in figures 2*b–d*.

In this and the following section we refer to the voltage coordinate of the EP as v_0, and the maximum voltage of the unstable limit cycle as v_{ulc}. Also f_{R} is the resonant frequency of the linearized equations at the EP and the f_{Th} is the frequency at which the (nonlinear) TC has its minimum value. Two interesting features of the TC are its sharp corner at f_{Th}, and its asymmetry. For frequencies just below f_{Th} the curve is parabolic. For frequencies just above f_{Th} the curve is steeper and almost linear, levelling off at $(f_{\mathrm{Th}} + 3)$ Hz in the example shown in figure 2a. This asymmetry in the responses is shown in figure 2*b–d*. Each of these figures shows the response of the system to a periodic input of amplitude $\bar{I} = 0.1\ \mu\mathrm{A\,cm^{-2}}$. In figure 2*b* the frequency is 35 Hz which as shown in figure 2*a* is just to the left of the TC. In figure 2*c* the frequency is 35.6 Hz just to the right of the TC. In figure 2*d* the frequency is 40 Hz just to the right of the TC on the steep right hand side. Here the maximum membrane potential oscillates below v_{ulc} and does not succeed in reaching the stable limit cycle. These asymmetric features will be explained below.

4. THE RESPONSE CURVE (RC)

In the previous section the response was described by giving the threshold amplitude of the input signal required to drive the system into its stable limit cycle for varying input frequency. The resulting curve was

PHILOSOPHICAL TRANSACTIONS OF THE ROYAL SOCIETY B BIOLOGICAL SCIENCES

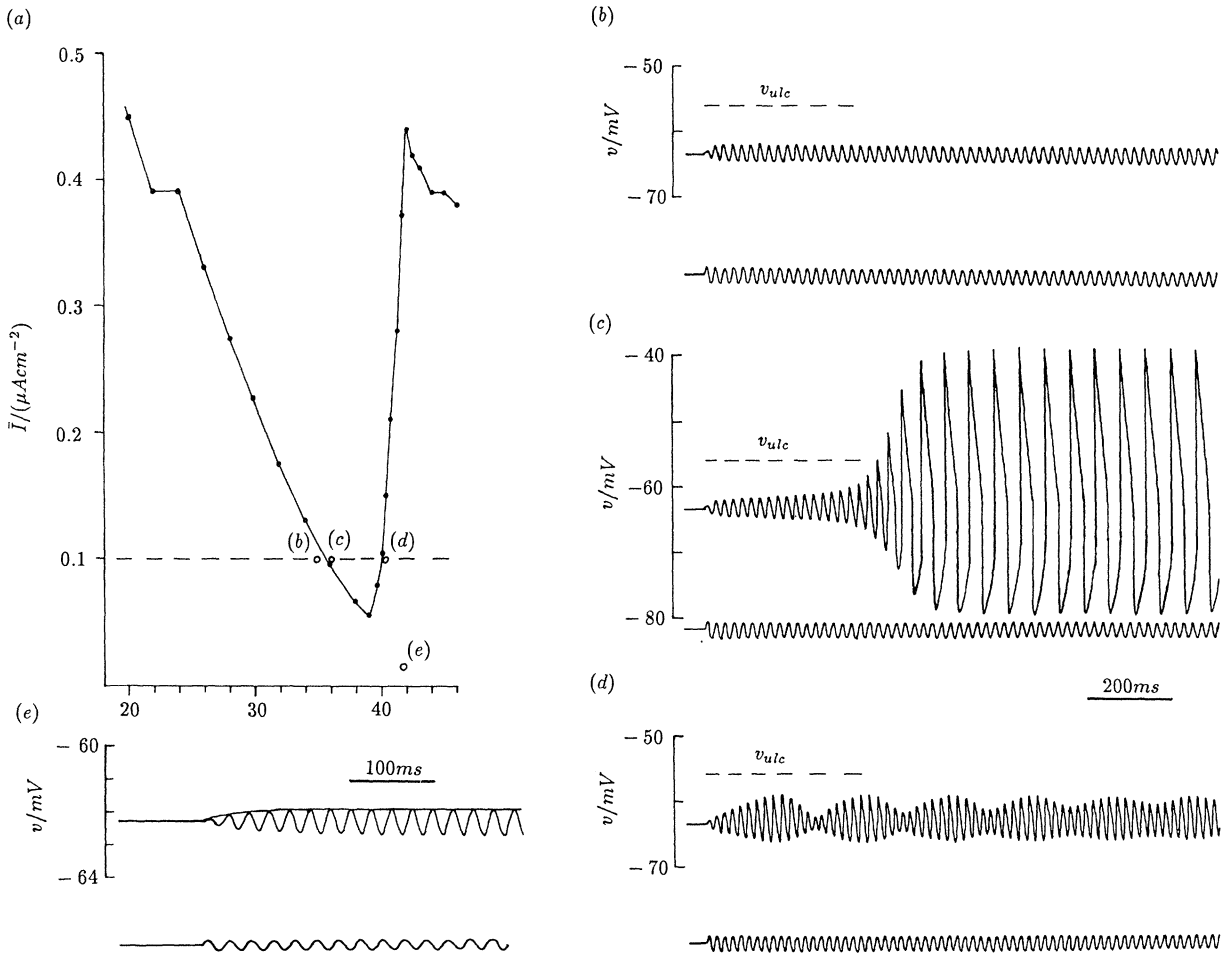

Figure 2. (*a*) Threshold curve (TC) for the standard model obtained by numerical integration of equations (3) at $v_0 = -63.3\,\text{mV}$ with $I_0 = -1.35\,\mu\text{A cm}^{-2}$ and $I = 0$. This graph shows the amplitude $\bar{I}$ of a periodic input $\bar{I}\cos\omega t$ which is just sufficient to drive the system into a stable limit cycle with $f = 1000\omega/(2\pi)\,\text{Hz}$. (*b–d*) are examples of voltage responses obtained by numerical integration of equations (3) for $\bar{I} = 0.1\,\mu\text{A cm}^{-2}$ (see horizontal dashed line in (*a*)) at frequencies: (*b*) $f = 35\,\text{Hz}$, (*c*) $f = 35.6\,\text{Hz}$ and (*d*) $f = 40\,\text{Hz}$. The stimulating current is shown below each trace, and the corresponding points with coordinates $(f, \bar{I})$ are indicated by the open circles labelled (*b*), (*c*) and (*d*) in (*a*). (*e*) Timecourse of voltage response for equations (3) with $f = 41.85\,\text{Hz}$ and $\bar{I} = 0.016\,\mu\text{A cm}^{-2}$. The growth in voltage amplitude shown by the solid curve was calculated from the averaged model of the model equations for small r as given by equation (7) in §6. This choice of $(f, \bar{I})$ values corresponds to the open circle labelled (*e*) in (*a*).

called the threshold curve (TC). An alternative way of describing the response is to give the output voltage amplitude for an input signal of fixed amplitude for varying frequencies. We refer to the latter as a response curve (RC).

Figure 3 shows the relationship between the TC shown in figure 2*a* (and reproduced in figure 3*a*), and the corresponding RCs (figure 3*b*). The RC for the linear approximation to equations (3) at the EP can be calculated analytically and is shown for $\bar{I} = 0.016\,\mu\text{A cm}^{-2}$ by the lower dotted curve in figure 3*b*. The shape of this linear RC is independent of the value of $\bar{I}$. Thus doubling the value of $\bar{I}$ to $0.032\,\mu\text{A cm}^{-2}$ doubles the amplitude of the linear RC (upper dotted curve in figure 3*b*).

The nonlinear RCs (solid curves of Figure 3*b*) were obtained by integrating equations (3) numerically for fixed values of $\bar{I}$, and measuring the amplitude of the voltage response over a range of frequencies. In this case the shape of the curve depends on the value of $\bar{I}$. Thus for $\bar{I} = 0.016\,\mu\text{A cm}^{-2}$ the nonlinear RC is hardly distinguishable from that of the linear RC (shown as a dotted curve in the lower part of figure 3*b*). When the value of $\bar{I}$ is doubled to $0.032\,\mu\text{A cm}^{-2}$ the nonlinear RC has a sharper peak than the corresponding linear RC (compare the almost coincident solid and dotted curves in the lower part of figure 3*b*). For amplitudes of $\bar{I}$ beyond $0.0345\,\mu\text{A cm}^{-2}$ the RCs steepen and terminate when the threshold amplitude is exceeded and the system enters its stable limit cycle.

Response curves have been described previously in cells such as the squid axon (Mauro *et al.* 1970; Fitzhugh 1983), frog node (Clapham & de Felice 1982), heart cell membrane (De Haan & De Felice 1978), and inner hair cells (Ashmore & Attwell 1985; Crawford & Fettiplace 1981). In our system (equations (3)) the presence of a firing threshold means that the response can be described in terms of either a TC or a set of RCs. In the next section we

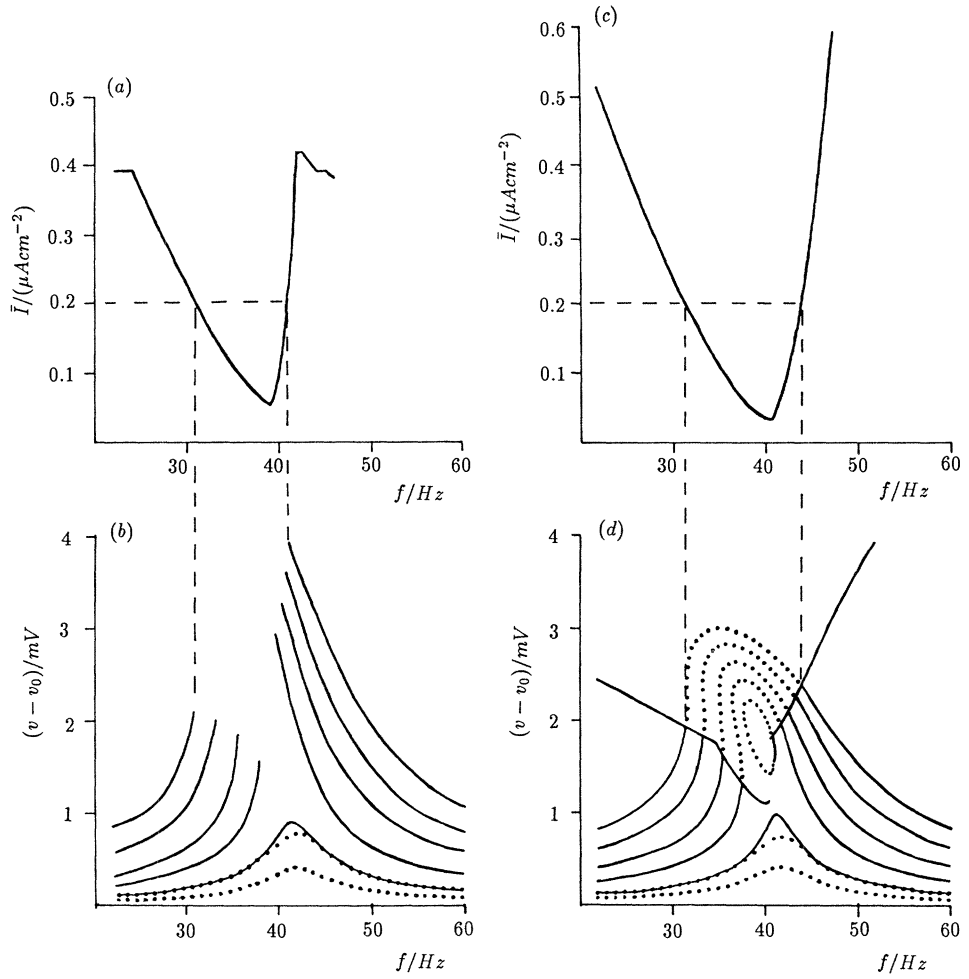

Figure 3. Comparison of (*a*) threshold curve (TC) and (*b*) response curves obtained numerically for the standard physiological model at $v_0 = -63.3$ mV, with (*c*) TC and (*d*) RCs obtained analytically for the averaged model of the model at the same EP. The TC in (*a*) is a reproduction of figure 2*a*. The TC in (*c*) is a reproduction of figure 4*a*. In (*b*) and (*d*) the two lower dotted RCs curves were obtained analytically for the linear approximation to equations (3) and (5) respectively for two values of $\bar{I} = 0.016\,\mu A\,cm^{-2}$ and $\bar{I} = 0.032\,\mu A\,cm^{-2}$. In (*b*) the five solid curves were obtained by numerical integration of equations (3) (physiological model) for $\bar{I} = 0.032$, 0.064, 0.1, 0.15 and $0.2\,\mu A\,cm^{-2}$. In (*d*) the five solid curves were obtained analytically (see § 7) for the model of the model with the same values of $\bar{I}$. Also shown in (*d*) are the threshold curves determined by the Routh conditions R2 and R3 (see § 7) which divide each RC into a section which is subthreshold (solid curve) and a section above threshold (shown dotted). Horizontal dashed lines at $\bar{I} = 0.2\,\mu A\,cm^{-2}$ in (*a*) and (*c*) intersect each TC at two points. These points are projected downwards in each case to meet the corresponding threshold points on the RCs for $\bar{I} = 0.2\,\mu A\,cm^{-2}$.

describe how the simpler model of the model of Hindmarsh & Rose (1994*a*) may be used to obtain analytically the TC and set of RCs shown in figures 3*c*,*d*.

5. THE RESPONSE TO PERIODIC CURRENT INPUTS

Equations (11) of Hindmarsh & Rose (1994*a*) are:

$$\dot{x} = -\alpha x + \beta y - \alpha(a(x^2 + y^2 - bz)x + T_{11}(I + I(t)),$$

$$\dot{y} = -\beta x - \alpha y - \alpha(a(x^2 + y^2 - bz)y + T_{21}(I + I(t)),$$

$$\dot{z} = -\gamma z + \gamma(c(x^2 + y^2 - d(x^2 + y^2)^2) + T_{31}(I + I(t)).$$

We will consider the case where $I(t) = \bar{I}\cos\omega t$. Changing coordinates using equations (13) of Hindmarsh & Rose (1994*a*) we get:

$$\dot{\bar{x}} = -\alpha\bar{x}\left(1 + a(\bar{x}^2 + \bar{y}^2) - b\left(\bar{z} + \frac{IT_{31}}{\gamma}\right)\right) + \beta\bar{y} + T_{11}\bar{I}\cos\omega t,$$

$$\dot{\bar{y}} = -\alpha\bar{y}\left(1 + a(\bar{x}^2 + \bar{y}^2) - b\left(\bar{z} + \frac{IT_{31}}{\gamma}\right)\right) - \beta\bar{x} + T_{21}\bar{I}\cos\omega t,$$

$$\dot{\bar{z}} = -\gamma(\bar{z} - c(\bar{x}^2 + \bar{y}^2) + d(\bar{x}^2 + \bar{y}^2)^2) + T_{31}\bar{I}\cos\omega t.$$

In polar coordinates these equations become:

$$\dot{\bar{r}} = -\alpha\bar{r}\left(1 + a\bar{r}^2 - b\left(\bar{z} + \frac{IT_{31}}{\gamma}\right)\right) + \bar{I}\cos\omega t(T_{11}\cos\theta + T_{21}\sin\theta),$$

$$\dot{\bar{\theta}} = -\beta + \frac{\bar{I}\cos\omega t(-T_{11}\sin\theta + T_{21}\cos\theta)}{\bar{r}},$$

$$\dot{\bar{z}} = -\gamma(\bar{z} - c\bar{r}^2 + d\bar{r}^4) + T_{31}\bar{I}\cos\omega t.$$

These equations may be written as:

$$\left.\begin{aligned}\dot{r} &= -\alpha r\left(1 + ar^2 - b\left(z + \frac{g}{\gamma}\right)\right) \\ &\quad + \bar{g}\cos\omega t\cos(\phi - \theta), \\ \dot{\theta} &= -\beta + \frac{\bar{g}\cos\omega t\sin(\phi - \theta)}{r}, \\ \dot{z} &= -\gamma(z - cr^2 + dr^4) + g\cos\omega t,\end{aligned}\right\} \tag{4}$$

where

$$g = IT_{31}, \quad \bar{g} = \bar{I}(T_{11}^2 + T_{21}^2)^{1/2},$$
$$\cos\phi = \frac{T_{11}}{(T_{11}^2 + T_{21}^2)^{1/2}}, \quad \sin\phi = \frac{T_{21}}{(T_{11}^2 + T_{21}^2)^{\frac{1}{2}}}.$$

At this stage is it necessary to modify the model of the model (equations (4)) in order to explain the asymmetry of the threshold curve. This asymmetry arises because the frequency of oscillation of the system at its unstable limit cycle is less than the frequency of oscillation near the EP. The frequency of oscillation of the system decreases with amplitude. This is also shown by the fact that the frequency of maximum response decreases as the driving amplitude (for subthreshold amplitudes) increases, as shown in figure 3*b*.

The modification we chose was to rewrite the $\dot{\theta}$ equation of equations (4) as:

$$\dot{\theta} = -\beta + er^2 + \frac{\bar{g}\cos\omega t\sin(\phi - \theta)}{r}.$$

The term er^2 was obtained by starting the system in a state near the unstable limit.cycle and integrating the physiological model equations (1). The timecourse of the membrane potential was plotted to measure the frequency of oscillation, and the timecourse of the radial coordinate of the polar form of the canonical coordinate system was plotted to measure the corresponding amplitude. In this way we found a suitable value of e to be 4000.

6. THE AVERAGED FORM OF THE MODEL OF THE MODEL EQUATIONS

Putting $\psi = \omega t - (\phi - \theta)$ and $\omega = \beta + \delta$, equations (4), modified as above, many be written as:

$$\dot{r} = -\alpha r(1 + ar^2 - b(z + g/\gamma)) + \frac{\bar{g}(\cos\psi + \cos(2\omega t - \psi))}{2},$$
$$\dot{\psi} = \delta + er^2 + \frac{\bar{g}(-\sin\psi + \sin(2\omega t - \psi))}{2r},$$
$$\dot{z} = -\gamma(z - cr^2 + dr^4) + g\cos\omega t.$$

The averaged version of these equations is obtained by ignoring $\cos(2\omega t - \psi)$, $\sin(2\omega t - \psi)$ and $\cos\omega t$ terms, and is,

$$\left.\begin{aligned}\dot{r} &= -\alpha r(1 + ar^2 - b(z + g/\gamma)) + \frac{\bar{g}(\cos\psi)}{2}, \\ \dot{\psi} &= \delta + er^2 - \frac{\bar{g}(\sin\psi)}{2r}, \\ \dot{z} &= -\gamma(z - cr^2 + dr^4).\end{aligned}\right\} \tag{5}$$

Our first use of these equations is to describe the growth in amplitude of the response of the system, started in equilibrium with $g = 0$, to a periodic input of subthreshold amplitude. For small r and at resonance, $\delta = 0$, and equations (5) become:

$$\left.\begin{aligned}\dot{r} &= -\alpha r + \frac{\bar{g}(\cos\psi)}{2}, \\ \dot{\psi} &= -\frac{\bar{g}(\sin\psi)}{2r}, \\ \dot{z} &= -\gamma z.\end{aligned}\right\} \tag{6}$$

Using the initial conditions that $\psi(0) = 0$, $z(0) = 0$ and $r(0) = \epsilon$ (small) we obtain:

$$\psi(t) = 0, \quad z(t) = 0,$$

and so

$$\dot{r} = -\alpha r + \frac{\bar{g}}{2},$$

from which

$$r(t) = \frac{\bar{g}}{2\alpha} + \left(\epsilon - \frac{\bar{g}}{2\alpha}\right)e^{-\alpha t}. \tag{7}$$

So, using the transformations (8), (9) and (14) of Hindmarsh & Rose (1994*a*), the membrane potential is given by:

$$v(t) = v_0 + T_{11}r(t)\cos(\theta(t)) + T_{12}r(t)\sin(\theta(t)) + T_{13}z(t).$$

Because

$$\theta(t) = \psi(t) - \omega t + \phi = \phi - \omega t,$$

and $T_{12} = 0$, the membrane potential is:

$$v(t) = v_0 + T_{11}r(t)\cos(\phi - \omega t),$$

an oscillation whose growth in amplitude is given by $T_{11}r(t)$.

For small values of $\bar{g}$, use of equations (7) gives an accurate fit to the transient time course of the membrane potential as shown in figure 2*e*.

By including δ in the $\dot{\psi}$ equation of equations (6), and putting $\dot{r} = \dot{\psi} = \dot{z} = 0$ we also obtain the steady state response for different values of δ:

$$r_{ss} = \frac{\bar{g}}{2}\sqrt{\left(\frac{1}{\alpha^2 + \delta^2}\right)}.$$

Using $v_{ss} = T_{11}r_{ss}$ this gives the dotted RCs in the lower part of figure 3*d* for two different values of $\bar{g}$. These curves can be compared to the dotted curves of the lower part of figure 3*b* which were obtained from the linear approximation of the physiological model (equations (3)) using the same values of $\bar{I}$ (or $\bar{g}$).

PHILOSOPHICAL TRANSACTIONS OF THE ROYAL SOCIETY B BIOLOGICAL SCIENCES

7. DERIVATION OF THE THRESHOLD CURVE

We will now use the averaged equations (5) to derive the threshold curve, and thereby see analytically the reason for the asymmetry and sharp corner at f_{Th}.

Behaviour near the unstable limit cycle is crucial in determining whether or not the system goes above threshold. For the cases we will consider, with small values of I, the unstable limit cycle is much smaller than the stable limit cycle (see figure 1*a*). By removing the term dr^4, responsible for the appearance of the stable limit cycle, we do not significantly affect the behaviour of the system near the unstable limit cycle. Without the term dr^4 the response of the system becomes unbounded once it is raised above threshold. We therefore make the following assumption. If, for given values of δ and $\bar{g}$, the system (5) does not have a stable EP, then the amplitude is above threshold.

The coordinates (r_0, ψ_0, z_0) of the EP of the equations (5) with $d = 0$ must satisfy:

$$\left.\begin{aligned} -\alpha r_0(1 + ar_0^2 - b(z_0 + g/\gamma)) + \bar{g}(\cos\psi_0)/2 = 0, \\ \delta + er_0^2 - \bar{g}(\sin\psi_0)/(2r_0) = 0, \\ -\gamma(z_0 - cr_0^2) = 0, \end{aligned}\right\} \quad (8)$$

so by elimination of ψ_0 and z_0, r_0 must satisfy:

$$\alpha^2 r^2((1 - bg/\gamma) + (a - bc)r^2)^2 + (\delta + er^2)^2 r^2 = \bar{g}^2/4. \quad (9)$$

The linear approximation at an EP (r_0, ψ_0, z_0) is:

$$\begin{pmatrix} \alpha(-(3a - bc)r_0^2 - (1 - bg/\gamma)) & -r_0(\delta + er_0^2) & \alpha b r_0 \\ (2er_0^2 + \delta + er_0^2)/r_0 & -\alpha((a - bc)r_0^2 + (1 - bg/\gamma)) & 0 \\ 2c\gamma r_0 & 0 & -\gamma \end{pmatrix},$$

where equations (8) have been used to express the partial derivatives in terms of r_0.

The eigenvalues of this matrix are the roots of the characteristic equation:

$$\lambda^3 + a_1(r_0^2)\lambda^2 + a_2(r_0^2)\lambda + a_3(r_0^2) = 0,$$

where

$$\begin{aligned} a_1(r_0^2) &= 2\alpha((1 - bg/\gamma) + (2a - bc)r_0^2) + \gamma, \\ a_2(r_0^2) &= 2\alpha\gamma((1 - bg/\gamma) + 2(a - bc)r_0^2) \\ &\quad + (\delta + er_0^2)(\delta + 3er_0^2) + \alpha^2((1 - bg/\gamma) \\ &\quad + (a - bc)r_0^2)((1 - bg/\gamma) + (3a - bc)r_0^2), \\ a_3(r_0^2) &= \alpha^2\gamma((1 - bg/\gamma) + (a - bc)r_0^2)((1 - bg/\gamma) \\ &\quad + 3(a - bc)r_0^2) + \gamma(\delta + er_0^2)(\delta + 3er_0^2). \end{aligned}$$

The Routh conditions for stability of the EP at (r_0, ψ_0, z_0) are that:

$$a_1(r_0^2) > 0, \quad (R1)$$

$$a_3(r_0^2) > 0, \quad (R2)$$

$$a_1(r_0^2)a_2(r_0^2) - a_3(r_0^2) > 0. \quad (R3)$$

For our parameter values $2a - bc > 0$, and so the first of these conditions is always satisfied when $0 \leqslant g \leqslant \gamma/b$.

For each pair $(\delta, \bar{g})$ we found all positive roots, r_0, of equation (9). If at least one of them gave a stable EP according to the Routh conditions, then according to our assumption above, that pair was below threshold. By converting the parameters δ and $\bar{g}$ into frequency $f = 1000(\beta + \delta)/(2\pi)$ and current amplitude $\bar{I} = \bar{g}/(T_{11}^2 + T_{21}^2)^{1/2}$ we obtain the TC for the averaged model of the model. This curve is shown in figure 4*a* (and reproduced in figure 3*c*) and exhibits the sharp corner and asymmetry that we noted in the physiological model (compare figures 3*a* and 3*c*).

To understand more clearly the shape of this threshold curve we will find the points $(\delta, \bar{g})$ in parameter space at which the individual Routh conditions fail. That is, the parameter values for which the system has an EP at (r_0, ψ_0, z_0) for which either

$$a_3(r_0^2) = 0, \quad (10)$$

or:

$$a_1(r_0^2)a_2(r_0^2) - a_3(r_0^2) = 0. \quad (11)$$

This is done by taking advantage of the fact that the Routh conditions are quadratic in δ and do not depend on $\bar{g}$. For each $r_0 \in [0, 0.05]$ we find the values of δ for which equation (10) holds. Then, for that r_0 and these values of δ, we find, using equation (9), the value of $\bar{g}$ which allows (r_0, ψ_0, z_0) to be an EP. These parameter values for which the system has an EP where equations (10) are satisfied are shown as the curve Routh 2 in figure 4*b*.

For the third Routh condition, R3, the parameter values for which the system has an EP, where equations (11) are satisfied, can be found in the same way. These values are shown as the curve Routh 3 in figure 4*b*.

The second Routh condition, R2, is simply the condition that the determinant of the linear approximation be greater than zero. Thus points on the curve Routh 2 are parameter values for which the system has an EP for which the determinant is zero. This EP has a zero eigenvalue and the system has a saddle-node bifurcation at such a point.

The number of EPs and their stability can change only at points in parameter space that lie on the curves Routh 2 or Routh 3 in figure 4*b*. Therefore by examining the system at one point in each region bounded by the curves in figure 4*b* we can determine the number of stable and unstable EPs in each such region. These numbers are shown in form $(\frac{n}{m})$ where n is the number of stable EPs and m is the number of unstable EPs. We note that the sharp corner results from the intersection of Routh 2 and Routh 3 and that

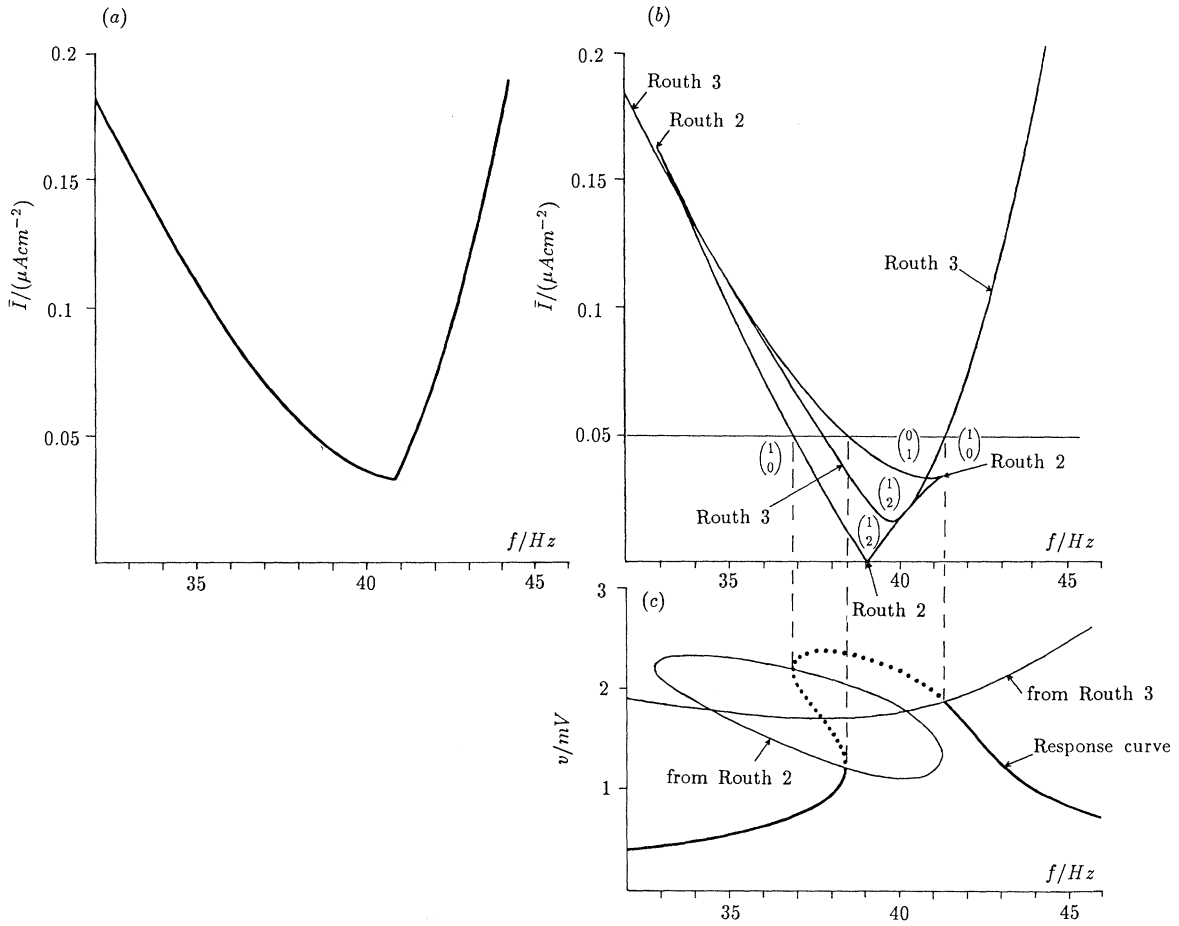

Figure 4. (*a*) The threshold curve obtained analytically for the model of the model (see § 7). (*b*) The curves Routh 2 and Routh 3 dividing the $(f, \bar{I})$ parameter space into regions, in which the number, n, of stable and number, m, of unstable EPs is shown as $\binom{n}{m}$. A horizontal line is drawn at $\bar{I} = 0.05\,\mu A\,cm^{-2}$. (*c*) The response curve for $\bar{I} = 0.05\,\mu A\,cm^{-2}$. Stable points shown by a continuous curve and unstable points shown by a dotted curve. Stability may change when the response curve crosses curves calculated from Routh 2 and Routh 3.

there is fine detail associated with the close proximity of these curves on the left-hand side. This detail was ignored in drawing figure 4*a*. Duffing type jump phenomena associated with the detail near the sharp corner on the right-hand side will be commented on below.

In figure 4*c* we show an RC for a particular value of $\bar{I}(\bar{g})$ for the averaged model of the model. This was calculated by finding all positive roots of equation (9) for that value of $\bar{g}$ and plotting:

$$v_{max} = v_0 + T_{11}^{-1}(x(I) + r_0) + T_{13}^{-1}(z(I) + z_0),$$

(see equations (22) of Hindmarsh & Rose (1994*a*)) against frequency. In this case $I = 0$ so $x(I) = 0 = z(I)$ and $z_0 = cr_0^2$ as we have ignored the term dr^4.

The Routh conditions R2 and R3 were used to determine the stability of points on the response curve. The relevant condition is indicated in figure 4*c*. These threshold curves divide the response curve into a section which is above threshold (shown dotted) and a section which is subthreshold (solid curve). Note that the frequencies at which the stability changes can be obtained from the top diagram by looking for the points where the horizontal line $\bar{I} = 0.05\,\mu A\,cm^{-2}$ $(\bar{g} = 0.00005)$ intersects the Routh condition curves.

Finally we show in figure 3*d* a set of RCs for varying $\bar{g}$ (or $\bar{I}$) for comparison with the physiological model using the same values of $\bar{I}$. These RCs resemble those of the Duffing equation shown in most standard textbooks on nonlinear dynamics, with the interesting variation that there are closed curves within the diagram. Together with the additional instabilities introduced by our notion of threshold, there is a greater variety of 'jump' phenomena than occurs with the Duffing equation. These jumps in the amplitude of the response occur as the frequency of the (constant amplitude) input is slowly changed. They may be regarded as a prediction of the model of the model about the behaviour of the physiological model. We have observed such jumps in the physiological model but the choice of the value of the amplitude of the input is so fine that it is unlikely that such jumps could be observed experimentally.

8. LIMITATIONS OF THE MODEL OF THE MODEL

In Figure 5 a logarithmic frequency scale is used to compare the TCs of the physiological model and the model of the model at low frequencies. The dotted

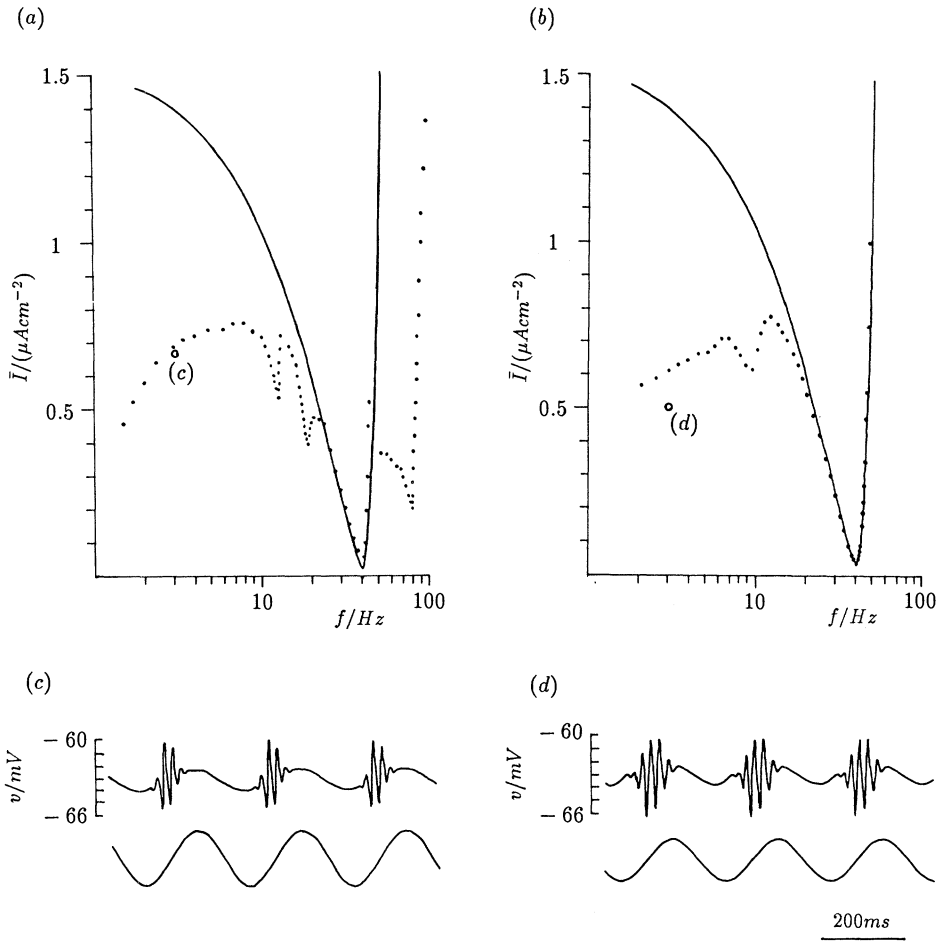

Figure 5. Threshold curves in low frequency range (logarithmic frequency scale) for (*a*) standard physiological model at $v_0 = -63.256$ mV, $I = 0$, $I_0 = -1.35\,\mu A\,cm^{-2}$ and (*b*) model of model at same EP. Dotted curves in (*a*) and (*b*) are threshold points obtained by numerical integration of equations (3) and equations (4) respectively. Solid curves in (*a*) and (*b*) were obtained analytically as described in the text. (*c*) Voltage response of physiological model at $f = 3$ Hz, $\bar{I} = 0.67\,\mu A\,cm^{-2}$ (point labelled (*c*) in (*a*)). (*d*) Voltage response obtained using model of model at $f = 3$ Hz, $\bar{I} = 0.5\,\mu A\,cm^{-2}$ (point labelled (*d*) in (*b*)).

curves in figure 5*a*,*b* were obtained by numerical integration of equations (3) (physiological model) and equations (4) (the model of the model) respectively. The solid curve in each case is the analytical TC obtained from the averaged model of the model equations as described above.

Although the numerical results shown in figure 5*a*,*b* are similar at low frequencies, it is clear that averaging does not apply below about 20 Hz. The reason for this is made clear by the examples shown in figure 5*c*,*d* for a representative point (open circle in figure 5*a*,*b*) in each model. Here the driving frequency is 3 Hz which is well below the natural frequency of the system.

9. THRESHOLD CURVES FOR DIFFERENT VALUES OF *I*

So far we have described the TC for the physiological model obtained numerically (figure 3*a*) and compared this with the TC obtained analytically for the averaged equations of the model of the model (figure 3*c*). In both cases $g = I/T_{31} = 0$, and the EP was very close to the bifurcation point (see figure 1*a*). In figure 6*a* we extend the range of frequencies to 100 Hz at the same EP ($I = 0$). As shown by the dotted curve, which was obtained by numerical integration of equations (3), the physiological model shows a prominent subharmonic at twice the resonant frequency (i.e. 78 Hz). This subharmonic is absent in the model of the model (see figure 5*b*) and in the analytical TC of the averaged model of the model equations (solid curve in figure 6*a*). We have not yet considered how to modify the model of the model to account for this subharmonic component.

An important question is to determine how these TCs change as the EP is moved further from bifurcation point. As the value of I is increased (figure 6*b*,*c*) the TC of the physiological model is displaced upwards and the subharmonic component becomes less prominent. The analytical TC (solid curve) is also displaced upwards as I is increased and appears to be related to the primary component of the physiological TC (with a minimum at f_{Th}). Note that this also means that if a RC was plotted for a fixed value of I, this RC would become reduced in amplitude as I was

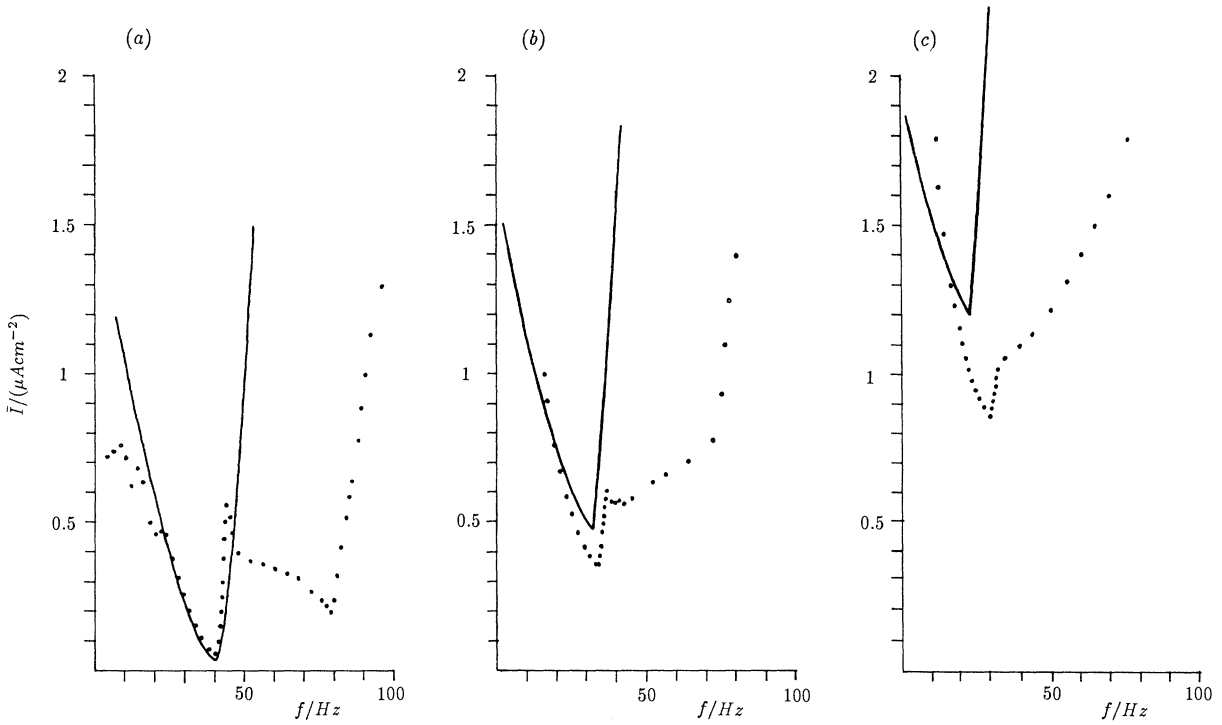

Figure 6. Threshold curves obtained numerically for the physiological model (dotted curves) and analytically for the averaged model of the model (solid curves) for (*a*) $I = 0\,\mu A\,cm^{-2}$, (*b*) $I = 0.35\,\mu A\,cm^{-2}$ and (*c*) $I = 0.7\,\mu A\,cm^{-2}$.

increased. This is the opposite of the change that occurs in the inner hair cells of lower vertebrates (Fettiplace 1987) where the RCs decrease in amplitude with steady hyperpolarization.

The Hodgkin–Huxley model also shows subthreshold oscillations and resonance which becomes more pronounced as the EP is brought closer to the boundary of stable and unstable region. (Hodgkin & Huxley 1952; Markevich & Sel'kov 1989), requiring fine adjustment of the external current to achieve resonance. This requirement for fine adjustment of the external current has previously been thought to suggest that resonance would be unlikely to be of physiological importance unless additional mechanisms could be found to improve the sharpness of the response curves (Markevich & Sel'kov 1989).

In mammalian neurons resonance may be of more significance than in the squid axon. Firstly, note that the three TCs of figure 6 were obtained at the three EPs for which we obtained the responses to pulses shown in figure 2. This means that although the differences in membrane potential are only of the order of 1.5 mV, EPs in this range span a considerable part of the bifurcation diagram (see figure 1*a*). In addition, the TCs were sharper than may have been expected given the degree of damping of the responses to these pulses. (Note that whereas the TCs were obtained from the model of the model which was constructed around the linear approximation at the EP with $I_0 = -1.35\,\mu A\,cm^{-2}$ the responses to pulses were obtained using the linear approximations at the three different EPs.) Secondly the asymmetry of the TC, in particular the steepness on the high frequency side of the resonance, means that the response of the cell is sensitive to small changes in driving frequency for frequencies just higher than resonance (one sided sharpness). Thirdly many mammalian neurons have additional ionic currents which are modulated by transmitters to slowly adjust the 'external current' (McCormick 1989). The additional complexity of the bifurcation diagram and the presence of these additional ionic currents suggests that resonance may be involved in synaptic transmission at certain relay nuclei of the mammalian brain.

10. EXPERIMENTAL VERIFICATION

In the previous paper (Hindmarsh & Rose 1994*a*) we showed that in the presence of tetrodotoxin (TTX) rebound bursting cells could be classified into four categories which we referred to as Types A, B, C and D. In this paper we have analysed resonance for a cell with a Type D bifurcation diagram. We now report the results of a numerical investigation of resonance in cells of Types A and B.

Figure 7*a* shows a rebound response to a hyperpolarizing current step for the four dimensional model discussed in the previous paper (Hindmarsh & Rose 1994*a*, equations (32)). The separation parameter, v_{sep}, has been chosen to be 2 mV to give a Type A bifurcation diagram (Hindmarsh & Rose 1994*a*, figure 10*a*). The external current is set to $0\,\mu A\,cm^{-2}$ and all other parameter values are given in Appendix 3 of Hindmarsh & Rose (1994*a*). As shown in figure 7*b*, in the presence of TTX the response to a hyperpolarizing current step is also a decaying oscillation. Recordings such as those shown in figure 7*a*,*b* are typical of a LHb neuron (Wilcox *et al.* 1988).

PHILOSOPHICAL TRANSACTIONS OF THE ROYAL SOCIETY B BIOLOGICAL SCIENCES

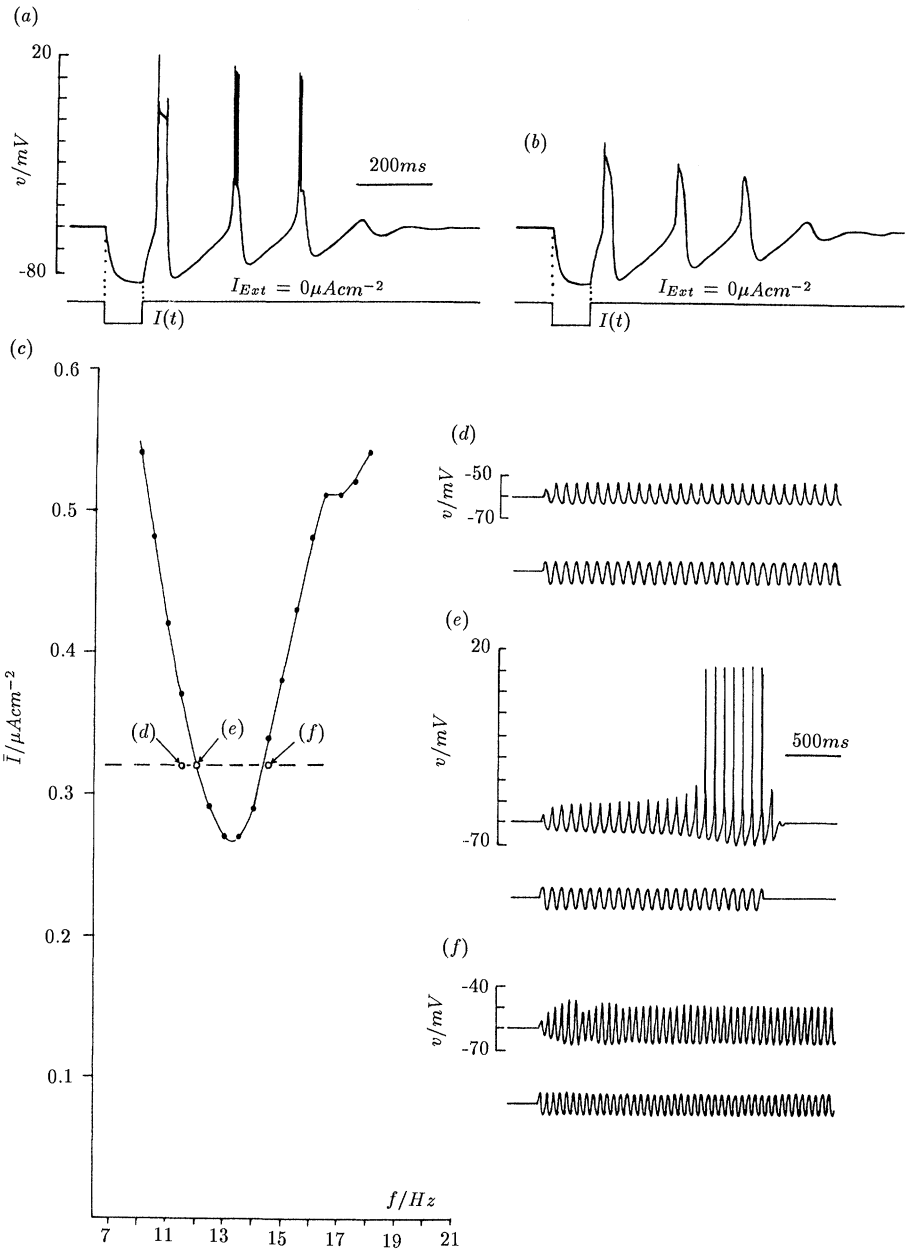

Figure 7. Predicted threshold curve for a cell with a Type A bifurcation diagram (e.g. a LHb neuron). (*a*) Response of the four-dimensional model, whose equations and parameter values are given in Appendix 3 of Hindmarsh & Rose (1994*a*), to a current step, $I(t)$, of amplitude $-3\,\mu A\,cm^{-2}$ and 50 ms in duration with $I_{Ext} = 0\,\mu A\,cm^{-2}$ and $v_{sep} = 2\,mV$. (*b*) Same numerical experiment as in (*a*) but in addition $g_{Na} = g_{NaP} = 0\,mS\,cm^{-2}$ to show how the cell would respond in the presence of TTX. (*c*) Threshold curve (TC) for the four-dimensional model with the same equations and parameter values as in (*a*). The graph shows the amplitude $\bar{I}$ of a periodic input $I(t) = \bar{I}\cos\omega t$ which is just sufficient to drive the system into bursting with $f = 1000/(2\pi)$ Hz. (*d–f*) Examples of voltage responses obtained by numerical integration of the four-dimensional model with the same equations and parameter values as in (*a*) for $\bar{I} = 0.32\,\mu A\,cm^{-2}$ (see horizontal dashed line in (*c*)) at frequencies (*d*) $f = 11$ Hz, (*e*) $f = 12$ Hz and (*f*) $f = 17$ Hz. The stimulating current is shown below each trace, and the corresponding points with coordinates $(f, \bar{I})$ are indicated by the open circles (*d*), (*e*) and (*f*) in (*c*).

We now construct a threshold tuning curve (TC) for this four-dimensional model. Although we do this numerically a similar procedure could be followed experimentally. We find for each value of the frequency, $f = 1000\omega/(2\pi)$ Hz, the (threshold) amplitude of a periodic input $I(t) = \bar{I}\cos\omega t$ which is just sufficient to drive the system from a stable EP to bursting. Note that previously our criterion for reaching threshold was that the cell went into low threshold oscillation. Here we require that the cell generates bursts of fast action potentials since this is easier to measure experimentally. The resulting TC is shown in figure 7*c*. Examples of reaching bursting for an input amplitude on the TC and failure to reach bursting for input amplitudes below the TC are shown in figure 7*d–f*. Note that in contrast to the responses to a Type D cell (figure 2*c*), firing stops when the periodic input is terminated (figure 7*e*).

Comparison of figure 7 with figure 2 shows that the TCs have similar features. In figure 2 the TC was parabolic for frequencies just below f_{Th} and more linear for frequencies just above f_{Th}. This asymmetry also occurs in figure 7 but is less pronounced. A clear indication of the asymmetry can be found by comparing figure 7*d*,*f* with figures 2*b*,*d*. In figure 7*d* the frequency is 11 Hz which is just to the left of the TC and the amplitude increases initially and is then constant. In figure 7*f* the frequency is 17 Hz which is just to the right of the TC and the maximum membrane potential oscillates slowly before settling down below threshold. This distinction between the left and right sides of the TC was also noted in figure 2.

In figure 8*a* we show a rebound response to a

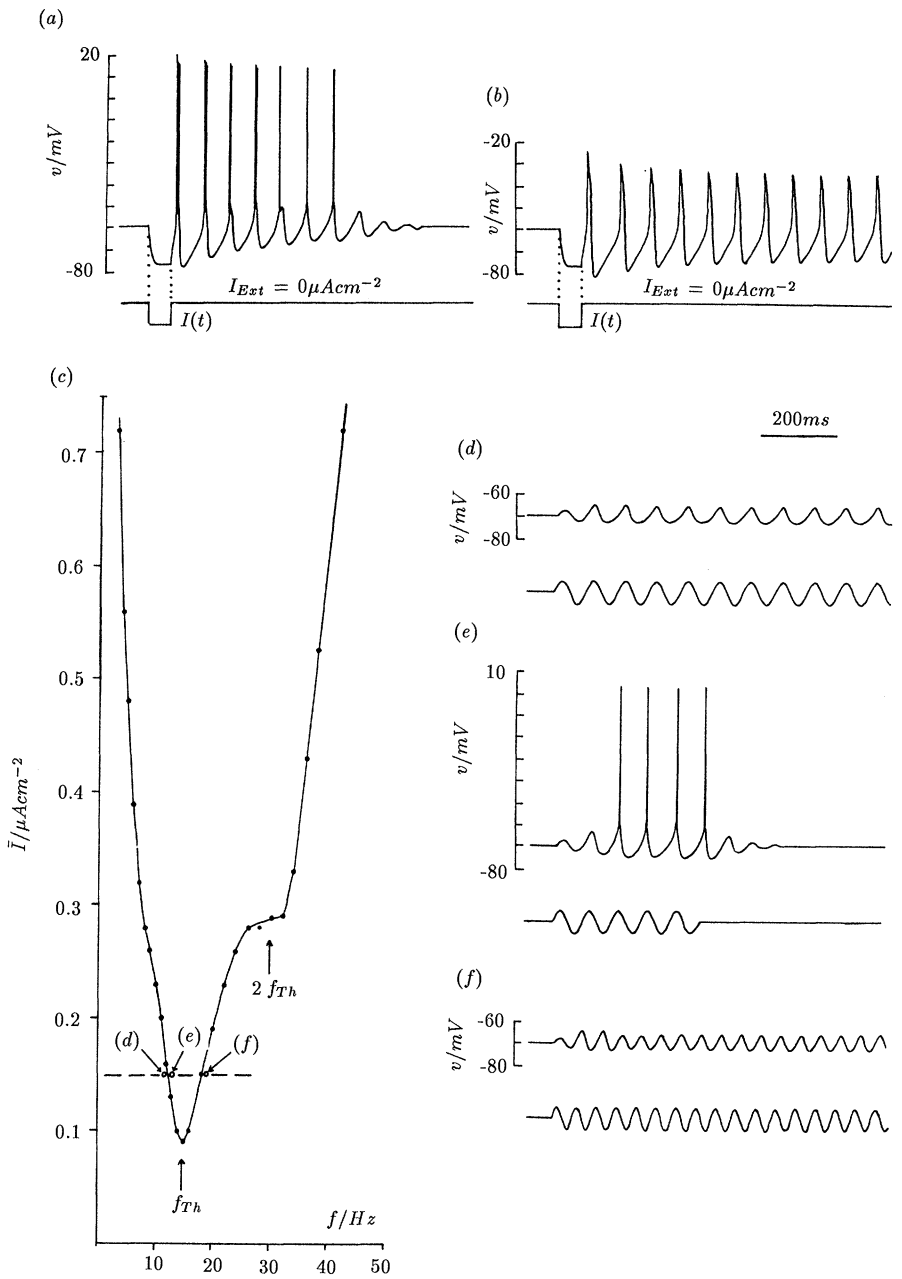

Figure 8. Predicted threshold curve for a cell with a Type B bifurcation diagram (e.g. some LHb neurons, some nRT neurons). (*a*) Response of the four-dimensional model, whose equations and parameter values are given in Appendix 3 of Hindmarsh & Rose (1994*a*), to a current step, $I(t)$, of amplitude $-2\,\mu\mathrm{A\,cm^{-2}}$ and 60 ms in duration with $I_{\mathrm{Ext}} = 0\,\mu\mathrm{A\,cm^{-2}}$ and $v_{\mathrm{sep}} = 1.45\,\mathrm{mV}$. (*b*) Same numerical experiment as in (*a*) but in addition $g_{\mathrm{Na}} = g_{\mathrm{NaP}} = 0\,\mathrm{mS\,cm^{-2}}$ to show how the cell would respond in the presence of TTX. (*c*) Threshold curve (TC) for the four-dimensional model with the same equations and parameter values as in (*a*). The graph shows the amplitude $\bar{I}$ of a periodic input $I(t) = \bar{I}\cos\omega t$ which is just sufficient to drive the system into bursting with $f = 1000/(2\pi)$ Hz. (*d*–*f*) Examples of voltage responses obtained by numerical integration of the four-dimensional model with the same equations and parameter values as in (*a*) for $\bar{I} = 0.15\,\mu\mathrm{A\,cm^{-2}}$ (see horizontal dashed line in (*c*)) at frequencies (*d*) $f = 12$ Hz, (*e*) $f = 13$ Hz and (*f*) $f = 19$ Hz. The stimulating current is shown below each trace, and the corresponding points with coordinates $(f, \bar{I})$ are indicated by the open circles (*d*), (*e*) and (*f*) in (*c*).

hyperpolarizing current step for the same four-dimensional model but with parameter values chosen to give our model of an nRT cell (see Appendix 3 of Hindmarsh & Rose (1994*a*)). The bifurcation diagram (with TTX) for these parameter values is shown in Figure 10*b* of Hindmarsh & Rose (1994*a*) and is of Type B. As we remarked in that paper the rebound response (without TTX) is a decaying oscillation with a tonic tail (figure 8*a*) whereas the oscillation is sustained in the presence of TTX (figure 8*b*).

The TC for this model is shown in figure 8*c*. Here the frequency range has been extended to 50 Hz to show the presence of a subharmonic at $2f_{\mathrm{Th}}$. The TC was calculated in the same way as in the previous example (figure 7*c*). Figure 8*d*–*f* shows representative examples of reaching bursting for an input amplitude above the TC and failure to reach bursting for input amplitudes below the TC. Note that in figure 8*e* bursting stops when the periodic input is terminated.

Thus we find that the predicted TCs for cells with bifurcation diagrams of Types A and B are similar to the TC for the Type D cell which we have described analytically.

11. CONCLUSIONS

To our knowledge this paper gives the first mathematical analysis of resonance for a model of a mammalian central neuron. We have predicted the responses to sinusoidal inputs for a class of mammalian neurons which show rebound bursting (Hindmarsh & Rose 1994*a*), of which lateral habenula neurons and neurons of the nucleus reticularis thalami are examples (see last section). Resonance has been described using a threshold tuning curve which could be measured experimentally. No experimental measurements of this type have so far been made on such cells. Note however that preliminary observations on inferior olivary cells (Llinás & Yarom 1986; Yarom 1991), which also show rebound bursting, have demonstrated the existence of resonant properties in these cells.

The tuning curve is asymmetrical. We are not aware of any other system for which an analytical explanation has been given for an asymmetrical tuning curve.

Although we have concentrated on the experimental measurement of resonance using sinusoidal inputs, it is likely that cells of this type will also show resonance under physiological conditions. Some preliminary numerical calculations for this type of input are included in the following paper (Hindmarsh & Rose 1994*b*).

In conclusion we add the following historical note. The possibility that central neurons may operate in the frequency domain rather than the time domain led Longuet-Higgins (1968) to apply holographic principles to the problem of storage and retrieval of temporal information. This idea was later considered to be unrealistic since it would require a bank of resonators each with a bandwidth of approximately 1 Hz (Longuet-Higgins 1989). The cells that we have described do have relatively narrow tuning curves and occur together in nuclei which could be considered as forming a filter bank. If experimental evidence for resonance could be obtained it would invite the reconsideration of the above ideas.

This work was supported by the Wellcome Trust.

REFERENCES

Ashmore, J.F. & Attwell, D. 1985 Models of electrical tuning in hair cells. *Proc. R. Soc. Lond.* B **226**, 325–344.

Chandler, W.K., Fitzhugh, R. & Cole, K.S. 1962 Theoretical stability properties of a space-clamped axon. *Biophys. J.* **2**, 105–127.

Clapham, D.E. & DeFelice, L.J. 1982 Small signal impedance of heart cell membranes. *J. Membr. Biol.* **67**, 63–71.

Crawford, A.C. & Fettiplace, R. 1981 An electrical tuning mechanism in turtle cochear hair cells. *J. Physiol., Lond.* **312**, 377–412.

De Haan, R.L. & DeFelice, L.J. 1978 Oscillatory properties and excitability of the heart cell membrane. *Theor. Chem.* **4**, 181–233.

Fitzhugh, R. 1983 Sinusoidal voltage clamp of the Hodgkin–Huxley model. *Biophys. J.* **42**, 11–16.

Hindmarsh, J.L. & Rose, R.M. 1994*a* A model for rebound bursting in mammalian neurons. *Phil. Trans. R. Soc. Lond.* B **346**, 129–150. (Preceding paper.)

Hindmarsh, J.L. & Rose, R.M. 1994*b* A model of intrinsic and driven spindling in thalamocortical neurons. *Phil. Trans. R. Soc. Lond.* B **346**, 165–183. (Following paper.)

Llinás, R.R. 1988 The intrinsic electrophysiological properties of mammalian neurons: insights into central nervous system function. *Science, Wash.* **242**, 1654–1664.

Llinás, R. & Yarom, Y. 1986 Oscillatory properties of guinea-pig inferior olivary neurons and their pharmacological modulation: *in vitro* study. *J. Physiol., Lond.* **376**, 163–182.

Longuet-Higgins, H.C. 1968 The non-local storage of temporal information. *Proc. R. Soc. Lond.* B **171**, 327–334.

Longuet-Higgins, H.C. 1989 A mechanism for the storage of temporal correlations. In *The computing neuron* (ed. R. Durbin, C. Miall & G. Mitchison), pp. 99–104. New York: Addison-Wesley.

Markevich, N.J. & Sel'kov, E.E. 1989 Parametric resonance and amplification in excitable membranes. The Hodgkin–Huxley model. *J. theor. Biol.* **140**, 27–38.

McCormick, D.A. 1989 Cholinergic and noradrenergic modulation of thalamocortical processing. *Trends Neurosci.* **12**, 215–221.

Mauro, A., Conti, F., Dodge, F. & Schor, R. 1970 Subthreshold behaviour and phenomenological impedance of the squid giant axon. *J. gen. Physiol.* **55**, 497–523.

Wilcox, K.S., Gutnick, M.J. & Christoph, G.R. 1988 Electrophysiological properties of neurons in the lateral habenula nucleus: an *in vitro* study. *J. Neurophysiol.* **59**, 212–225.

Yarom, Y. 1991 Rhythmogenesis in a hybrid system – interconnecting an olivary neuron to an analog network of coupled oscillators. *Neuroscience* **44**, 263–275.

Received 3 February 1994; accepted 3 May 1994

PHILOSOPHICAL TRANSACTIONS OF THE ROYAL SOCIETY B BIOLOGICAL SCIENCES